An optimized fringe tracker for the VLTI/PRIMA instrument

Frédéric Cassaing*[a], Bruno Fleury[a], Christophe Coudrain[a], Pierre-Yves Madec[a],
Emmanuel Di Folco[ab], Andreas Glindemann[b], Samuel Lévêque[b]

[a]Office National d'Études et de Recherches Aérospatiales,
Département d'Optique Théorique et Appliquée, BP 72, F-92322 CHATILLON

[b]European Southern Observatory, VLTI Group, D-85748 GARCHING BEI MUNCHEN

ABSTRACT

This paper presents new concepts for a Fringe Sensor Unit (FSU) optimized for high accuracy and low flux operation. This concept has been studied for the VLTI/PRIMA instrument in the H (and K) bands. To optimize both photon use and accuracy, an efficient spatial achromatic discrete modulation is chosen. For optical path difference measurements, most of the photons are used in a single polychromatic quadrature while the adjustable remaining part is dispersed for simultaneous group delay tracking. Integration time can be very short since no moving device is used. This FSU can also be turned to a classical two quadratures FSU if needed, for differential delay or visibility measurements. Optical designs for these FSUs are proposed. These simple designs are also very well suited to future space instruments. Theoretical performance and simulation results are finally given and compared to other existing devices.

Keywords: stellar speckle interferometry, interferometry, phase measurements, phase modulation, astronomical optics

INTRODUCTION

Interferometric combination of optical telescopes is now a validated technique for milli–arcsecond astronomy [1]. On the ground, performance of stellar interferometers is limited by the random optical path difference (OPD) introduced by atmospheric turbulence, reducing the magnitude of observable sources. The next frontier is to go faint: interferometers under construction include large telescopes corrected in the near infra–red with adaptive optics (AO) [2].

Unlike conventional telescopes, stellar interferometers do not deliver images but parameters such as visibilities, phase closures or group delay, measured by a Fringe Sensor Unit (FSU). Two kinds of FSU should be distinguished since, as in AO, performance can be increased by measuring stellar parameters in a long exposure Scientific Instrument (SI), while the interferogram is stabilized by an optical delay–line driven by an OPD Sensor (OS) measuring the OPD between the telescopes in a short exposure mode (fig. 1).

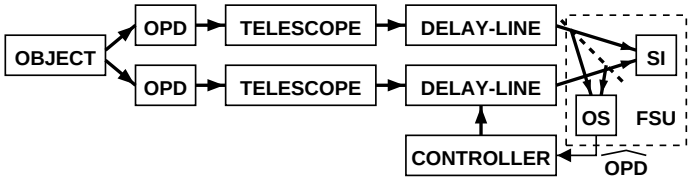

Figure 1. Layout of a stellar interferometer.

In most stellar interferometers, the SI and the OS are merged in the same FSU [3–5]. For the Very Large Telescope Interferometer (VLTI) of the European Southern Observatory (ESO), several SIs are foreseen operating in the I, J, H, K, L or M bands and provided by different institutes [6]. ESO has thus decided to include in the VLTI a dedicated OS, operating in the H and/or K bands. This OS is fed by the same object than the SI, or by a bright reference star located in the OPD isoplanatic patch within PRIMA (Phase Referenced Imaging and Micro-arcsec Astrometry) [7].

[1]Correpondance: E-mail: cassaing@onera.fr

The work reported here is derived from the feasibility study performed at ONERA for the VLTI FSU to be installed at Paranal. Tight specifications where given for this FSU, to be mostly used as an OS. Since the only requirements for an OS are fringe detection, centering and tracking, optimized OSs can give better results than estimating the OPD as a byproduct of a SI [8,9]. In section 1, a list of requirements for a perfect two–beam FSU is established from all the issues to address in stellar interferometry. Based on this analysis, a new simple and compact OS is proposed in section 2. Extension to a SI or more beams are also addressed. These designs are compared to a classical design in section 3.

1. FRINGE SENSING IN STELLAR INTERFEROMETRY

1.1. Modulation and demodulation

Monochromatic fringes are first considered. In a computer–based system, each intensity sample I_k of the interferogram measured at a phase offset Φ_k is given by:

$$I_k = (N/K)\,[1 + V\sin(\Phi + \Phi_\mathrm{r} + \Phi_k)] \tag{1}$$

$$\text{with} \quad \Phi = \Phi_\mathrm{a} + \Phi_\mathrm{i}, \tag{2}$$

where N is the total number of photons collected during the K samples of the measurement, V is the visibility, Φ_r is a known instrumental phase detailed in appendix A and Φ is the unknown sum of the phase Φ_a introduced by atmospheric turbulence and the phase Φ_i inside the instrument. To estimate the unknown parameters N, V and Φ, an additional known phase modulation $\Phi_\mathrm{m} = \{\Phi_k\}$ is introduced in the interferometer and the resulting intensity synchronously demodulated. Developping Eq. (1) shows that the modulated intensity can be decomposed on three known waveforms, a constant intensity offset and two quadratures $\cos(\Phi_\mathrm{r} + \Phi_\mathrm{m})$ and $\sin(\Phi_\mathrm{r} + \Phi_\mathrm{m})$, with respective coefficients N, $NV\sin\Phi$ and $NV\cos\Phi$. By linear demodulation, these three components can be derived from at least $K \geq 3$ intensity samples I_k, allowing easy estimation of the fringe parameters N, V and Φ (modulo 2π). Since the reference phase Φ_r (0 or $\pi/2$) just swaps quadratures, sin fringes (Φ_r=0) are assumed in the following.

The simplest and most used algorithm is based on a linear modulation of amplitude 2π ($\Phi_k = 2\pi k/K$). Taking advantage of the trigonometric shape of the interferogram, the K intensity samples are processed with a Digital Fourier Transform (DFT_K). In the well known case of the DFT_4 algorithm (fig. 2), with four intensity samples classically named A, B, C and D [3], the quadratures are simply $A - C$ and $B - D$ and the phase estimator is:

$$\widehat{\Phi} \equiv \arctan\left(\frac{A - C}{B - D}\right). \tag{3}$$

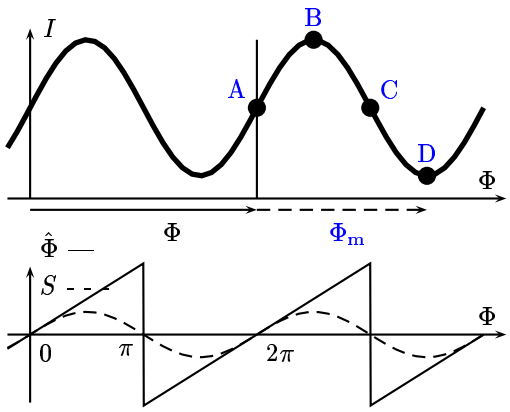

Figure 2. Monochromatic interferogram (top) and estimated phase (bottom) with $\mathrm{DFT}_{K\geq 3}$ (solid) and DFT_2 (dashed) algorithms.

When locked at Φ=0, the sine quadrature $A - C \propto NV\sin\Phi$ is the error signal, whereas the cosine quadrature $B - D \propto NV\cos\Phi \simeq NV$ is the fringe amplitude, used as a normalization factor. Another normalization is to divide

by $A+C \propto N$. We will call DFT_2 the degenerated algorithm based on a $\{0,\pi\}$ modulation and a single quadrature demodulation:

$$S \equiv \frac{A-C}{A+C} = V \sin\Phi. \tag{4}$$

Fig. 2 shows that S, derived from only two intensity samples, can be used for phase tracking at Φ=0. The linear range can be extended to $[-\pi/2,+\pi/2]$ using $\widehat{\Phi} \equiv \arcsin(S/V)$ if V is known.

Performance of demodulation algorithms is given by noise propagation. For an OS, the figure of merit is the variance of the phase estimator $\sigma^2(\widehat{\Phi})$ at Φ=0. For any algorithm, if the detector noise σ_e is expressed in number of photo–events [9]:

$$\sigma^2(\widehat{\Phi})\big|_{\Phi=0} \simeq \frac{P_S^2(N+K\sigma_e^2)}{N^2V^2}, \tag{5}$$

where P_S is a noise propagation coefficient for the sine quadrature, depending on the algorithm, through the choice of the modulation Φ_m and of the demodulation coefficients. For an OS, the goal is to minimize P_S. It can be shown [9] that the minimum value P_S=1 is reached for the DFT_2 algorithm, whereas $P_S=\sqrt{2}$ for $\mathrm{DFT}_{K\geq 3}$. This results from the fact that for a DFT_2 algorithm locked at Φ=0, all the photons are used where the slope is maximum whereas they are split in two quadratures in $\mathrm{DFT}_{K\geq 3}$ algorithms. With small residuals, an OS should therefore use the DFT_2 algorithm for best tracking. For open–loop measurements, the figure of merit is the variance of the visibility or phase estimators, averaged over all Φ values. It can be shown that the best algorithm is the DFT_K algorithm [9], with K=3 or 4 to minimize detector noise.

A discrete modulation, *i. e.* made of K phase steps Φ_k, was previously assumed. With usual continuous modulations, each sample results from a detector averaging while Φ_m is temporally or spatially varied. The interferogram visibility V derived from the object visibility V_0 is thus reduced by this blur. For DFT_K algorithms, the visibility loss is:

$$\eta_\mathrm{m} = \mathrm{sinc}\left(K^{-1}\right) \qquad \text{where } \mathrm{sinc}\,(x) = \sin(\pi x)/(\pi x). \tag{6}$$

Eq. (5) shows that this loss increases phase noise. Therefore, in the photon noise regime ($N > K\sigma_e^2$), where $\sigma^2(\widehat{\Phi}) \propto N^{-1}$ is independent of K, a high K value should be used with a continuous modulation to maximize η_m [8]. But in the detector noise regime ($N < K\sigma_e^2$), where a small K is required since $\sigma^2(\widehat{\Phi}) \propto K\,N^{-2}$, the modulation Φ_m should be discrete (η_m=1 instead of 0.9 for a continuous modulation with K=4).

1.2. Cophasing and coherencing

With polychromatic fringes, the phase Φ_a induced by an atmospheric OPD L_a is chromatic since for each monochromatic component of wavenumber $\sigma \equiv 1/\lambda$:

$$\Phi_\mathrm{a}(L_\mathrm{a},\sigma) = 2\pi\, L_\mathrm{a}\sigma. \tag{7}$$

Chromatic phase shifts can also occur in the modulation Φ_m since most modulation schemes modify the OPD between the beams, or in Φ_i with differential paths in air–filled delay–lines [10].

For a centro–symmetric star and without instrumental chromatism, all the spectral components are in phase on the central fringe defined by $L_\mathrm{a} = 0$. Assuming that these components have the same intensity and visibility in a spectral band $[\sigma_1,\sigma_2]$, Eq. (1) turns to a polychromatic interferogram:

$$I_k = (N/K)[1 + V\eta_\mathrm{c}\sin(2\pi\sigma_0 L_\mathrm{a})] \qquad \eta_\mathrm{c} = \mathrm{sinc}\,(L_\mathrm{a}/L_c)\,, \tag{8}$$

where the central wavenumber is $\sigma_0 = (\sigma_1+\sigma_2)/2$ and the chromatic envelope has a width $L_c = (\sigma_2-\sigma_1)^{-1} \simeq \lambda_0^2/\Delta\lambda$.

The best strategy to minimize detector noise in an OS is a wide band detection of the interferogram. With a small amplitude modulation ($\simeq \lambda_0$), neglecting the chromatic envelope, the interferogram is usually approximated by Eq. (1) with a local visibility. In this "cophasing" mode, tracking can occur at any integer multiple of λ_0 (fig. 3a, continuous line).

However, this scheme has a few drawbacks. First, using OPD modulation, the modulation amplitude must be adjusted to σ_0 which changes with the object spectrum. An achromatic phase modulation, *i. e.* such that the phase $\Phi_{\rm m}$, but not the OPD, is the same for all wavelengths is best suited. Second, the turbulent atmospheric OPD to correct can reach several tens of fringes. The amount of OPD residuals is given by the temporal band–pass of the controller (fig. 1), typically an integrator with adjustable gain. Optimum tracking results from a compromise between the atmospheric OPD and the measurement noise given by Eq. (5) [8, 11]. In case of poor conditions (faint object, low visibility, strong OPD fluctuations), fringe jumps may occur, leading the tracker to lose the null delay or even the fringe pattern.

To ensure central fringe tracking, visibility monitoring can be considered. But an unwrapped OPD estimator should be preferred (fig. 3a, dotted–dashed line) since a visibility reduction can result either from a left or right fringe jump, either from noise or turbulence fluctuations. In this "coherencing" mode, the incoming atmospheric OPD is reduced even if the residual OPD is larger than λ_0 (RMS), increasing performance of a short–exposure SI based on speckle techniques. Most coherencing algorithms are based on spectral dispersion of the interferometer output(s) on K' spectral channels. Achromatic modulation is supposed in the following, to avoid using a dedicated demodulation algorithm in each spectral channel [5], less efficient than the DFT algorithm.

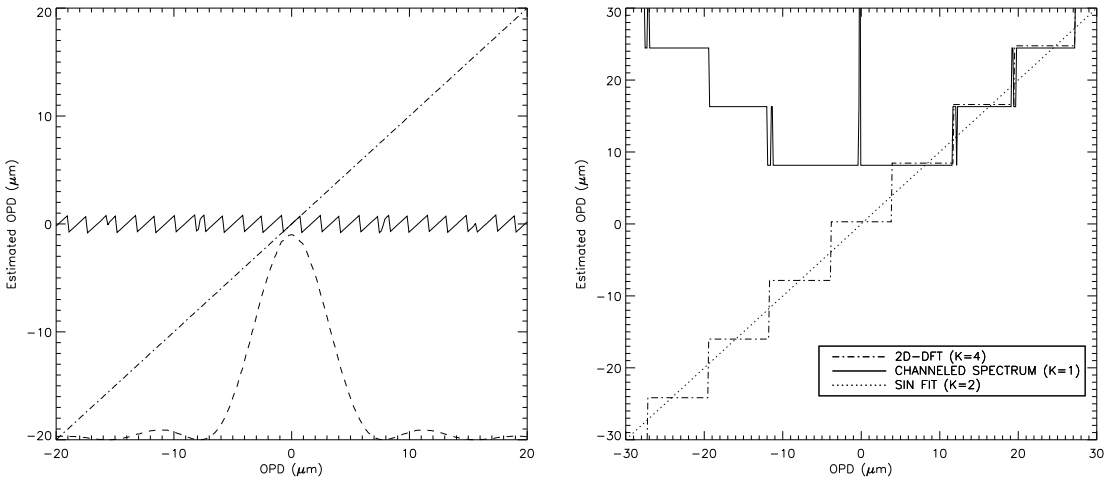

Figure 3. Demodulation of a polychromatic interferogram in the H band. a) DFT_4 algorithm, with visibility (- - -, arbitrary scale) and estimated OPD in the cophasing mode (—) and with spectral resolution using Eq. (9) (- . -). b) $\mathrm{DFT}_{K,K'}$ algorithm in the coherencing mode. See text for details.

A first coherencing algorithm is spectrally resolved demodulation. Assuming a linear 2π phase modulation with K steps in each channel, the interferogram is a $K' \times K$ bidimensional image. From the phases $\Phi(\sigma)$ measured with DFT_K in each spectral channel and assuming negligible chromatism, Eq. (7) shows that the atmospheric OPD can be estimated with

$$\widehat{OPD} = \frac{1}{2\pi}\frac{\partial\Phi(\sigma)}{\partial\sigma}. \tag{9}$$

With this algorithm (fig. 3a, dotted–dashed line), $\Phi(\sigma)$ must be unwrapped before derivation. Therefore, if there is too much noise for a wide band cophasing algorithm, phases $\Phi(\sigma)$ measured in smaller chromatic channels will be even more corrupted by noise and unwrapping will fail.

Unwrapping can be avoided by a joint bidimensional demodulation. Eq. (7) shows that Φ is linear with σ. It is thus possible to use spectral modulation, assuming same fringe parameters at each wavelength, exactly as we did in section 1.1 for phase modulation. The 2D Fourier Transform ($\mathrm{DFT}_{K,K'}$) of the interferogram is made of a central peak (the continuous term) and two fringe peaks (fig. 4a) whose position is related to the OPD [12]. The position of the closest pixel gives the OPD with a granularity equal to the coherence length (fig. 3b, dotted–dashed line). A

degenerated case is the well known "channeled spectrum" algorithm [13], based on the dispersion of a single output of the interferometer without phase modulation (fig. 4b, K=1). This algorithm, only estimating –in its classical form– $|L_a|$ (fig. 3b, continuous line) must be operated at $L_a \simeq K' L_c/2$, reducing visibility and dynamic.

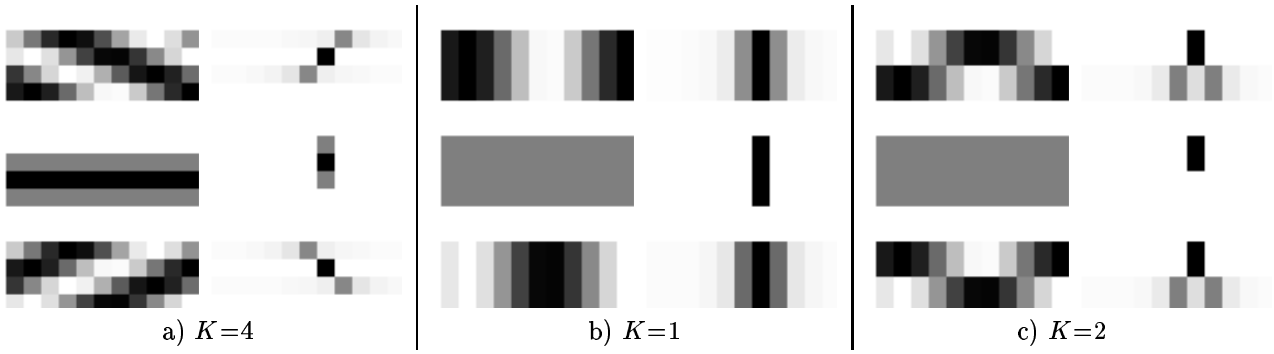

a) K=4 b) K=1 c) K=2

Figure 4. Bidimensional interferograms (left) and their $\mathrm{DFT}_{K,K'}$ spectrum (right) for three K values and OPD=+5 μm (top), 0, -5 μm (bottom). Horizontal: chromatic coordinate σ (K' values). Vertical: achromatic modulation coordinate Φ_m (K values).

1.3. Need and effect of spatial filtering

The OPD between the telescopes is the main but not the only aberration to compensate for in stellar interferometry. Interferograms can also be biased by aberrations and scintillation.

Atmospheric turbulence and static aberrations reduce the coherence over each pupil. Even with AO on each telescope, performance of stellar interferometers can be limited by AO residuals since correction is always partial [14]. But in stellar interferometry, the observed object is most often unresolved by each telescope. Coherence in the pupil of each telescope can thus be enhanced by filtering out the light outside the central core of the focal image [15]. Filtering with pin–holes does not modify the amplitude or phase of the part of the beam passing through. Some AO residuals are thus still present after filtering. Moreover, the size of the pin–hole should vary with the wavelength to match the diffraction spot. With mono–mode guides such as fibers [16] or planar integrated optics [17], a true modal filtering occurs [18] since exiting beams have a perfectly defined shape, allowing efficient beam combination and calibration [15, 19]. Moreover, the size of the guided mode is roughly proportional to λ. Most interferometers now plan to use spatial filtering.

Scintillation, increased by filtering, induce a visibility loss. With beams of unequal intensity N_1 and N_2:

$$\eta_s = \frac{2\sqrt{N_1 N_2}}{N_1 + N_2}. \tag{10}$$

Monitoring of η_s is required for accurate visibility measurements [15]. For an OS with spatial modulation, the phase is unaffected but visibility fluctuations impact on the noise of the estimated phase according to Eq. (5). The OPD controller should then be tuned according to $V = \eta_s V_0$, N and the OPD amplitude, as explained in section 1.2. Weighting with N is easy, and with full demodulation (*i. e.* with two quadratures), any function of V can be used. With the DFT_2 algorithm, V is not derived but S=$V \sin\Phi$ intrinsicly includes a linear weighting with η_s. This should be sufficient for simple control. Moreover, scintillation (or OPD residuals) induced cross–talk with temporal modulation. This can be reduced by increasing the modulation frequency, but in a detector–noise regime spatial modulation should be preferred [8].

Therefore, spatial filtering with mono–mode guides is the most efficient for a wide band stellar interferometer. AO residuals are converted into fast temporal fluctuation of the complex amplitude in each arm, *i. e.* intensity and phase. The SI and the OS should thus use the same spatial filter to see the same OPD [18]. Guided propagation also raises differential chromatism, polarization and instrumental OPD issues. Even-though these effects can be passively or actively controlled, a simple way to get rid of them is to filter after beam combination since filtering and combining operators commute and photometric channels, measuring N_1 and N_2 before combination to estimate η_s [15, 19] are not required for an OS, as long as a simple temporal controller is used.

2. DESIGN OF NEW OSS AND SIS

A classical concept FSU_0 is first reminded in section 2.1. A new OS FSU_1 is proposed in section 2.2, based on algorithms described in section 2.3. Extension to a SI (FSU_2) or more beams are addressed in sections 2.4 and 2.5. Performance of these design is evaluated in section 3.

2.1. The classical FSU_0 concept (OS & SI)

Most stellar interferometers use a similar concept we will call FSU_0 [3–5, 8, 20]. This concept depicted in fig. 5 is based on a Beam Splitter (BS) with a continuous temporal OPD modulation in one arm. The two BS outputs are most often considered as two distinct interferometers with full demodulation, operated in parallel and fed by half of the light. One is usually dedicated to a polychromatic cophasing OS, while the other is used as a spectrally resolved SI also providing coherencing. The OS and the SI have thus the same modulation frequency, increasing detector noise in the short–exposure SI. Moreover, the spectral resolution of the coherencing mode and the SI are the same.

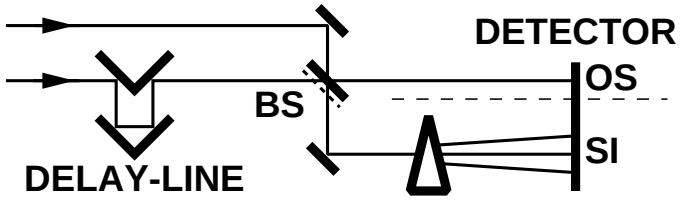

Figure 5. Principle of the concept FSU_0. See text for abbreviations.

Calibration is an important issue for a FSU. For FSU_0, the critical point is the precision of the delay–line modulation. Photometric calibration is relaxed since the K samples follow the same path.

2.2. The new FSU_1 concept (OS)

Section 1 has shown that an ideal cophasing OS should use the DFT_2 algorithm in a polychromatic channel with an achromatic discrete spatial modulation. A small part of the light should be dispersed to correct for possible fringe jumps, ensuring tracking of the central fringe. In a pure coherencing mode, all the light should be sent to the dispersed channels.

Spatial modulation is often associated with wavefront combination ("Young" fringes, fig. 11a). The modulation is then continuous and chromatic and the interferogram is modulated by the diffraction pattern of each aperture. Another solution is to consider the two complementary outputs of a BS as a $\{0, \pi\}$ spatial discrete modulation [9, 21]. Moreover, as explained in appendix A, a perfect BS leads to achromatic sine fringes as required since stellar interferometers are based on wavefront division at input. Joint use of the two outputs, in addition to temporal modulation, is used to increase the SNR by the FLUOR experiment [19].

All these requirements lead to the FSU_1 design detailed in fig. 6. In the cophasing mode, a large part of the light (α=90% for example) is used in a wide band polychromatic channel while the remaining part ($\beta = 1 - \alpha$) is dispersed for simultaneous coherencing control, at a lower frequency. For pure coherencing, β=1.

Calibration of FSU_1 is critical since each sample I_k results from a different path, requiring accurate characterization of each detector pixel, of each arm transmission in (fiber alignment). Moreover, real BS have some absorption: the two outputs are not exactly complementary. However, this effect can be calibrated for a cophasing OS locked at Φ=0 or neglected for a coherencing OS with significant OPD residuals. Calibration can be done by alternatively masking each beam or by using the external delay–lines (fig. 1) before tracking to cross–check spatial and temporal modulations. An internal calibration source can also be used, based on wavefront division to reproduce stellar sine fringes since appendix A shows that a double pass through the BS leads to cosine fringes. This has little impact in the cophasing mode ($\lambda_0/4$ OPD shift) but fig. 11c shows that if the interferogram is even, L_a sign cannot be derived from cosine fringes. Coherencing at L_a=0 with just two dispersed outputs is then impossible without an additional phase modulation.

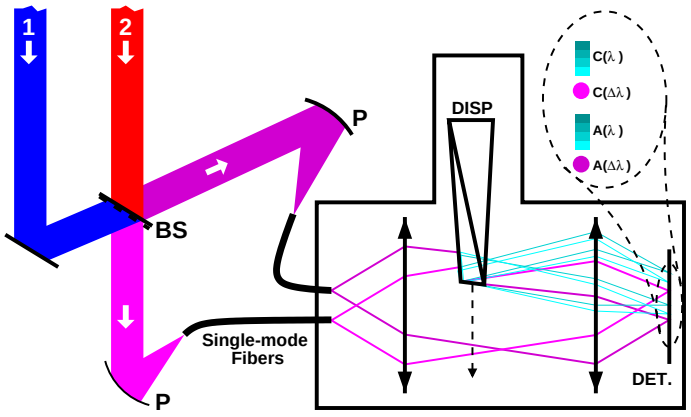

Figure 6. FSU_1 concept: the two outputs of the Beam Splitter BS are focused on a detector array with off–axis parabolae P through single–mode fibers and relay optics. In the intermediate collimated space, a prism assembly can disperse with small–deviation an adjustable part α of the light.

2.3. Single quadrature fringe detection and coherencing

Efficient fringe tracking is the main requirement for an OS but other features such as fringe detection, visibility estimation to calibrate the multiplicative constant in Eq. (4) or dispersion measurement to ensure that all the chromatic components are in phase, may also be required. We show in this subsection that FSU_1 can perform these measurements although they require two quadrature demodulation. Coherencing with a spectrally–resolved $\{0, \pi\}$ modulation, never investigated to the best of our knowledge, is also addressed.

The fact is that these additional measurements do not require extreme accuracy and are only required before tracking, or every few minutes, when the SI can be temporarily stopped. Like wings of an airplane are optimized for cruise flight and use high–lift flaps for take–off and landing, FSU_1 is optimized for tracking but can use an additional temporal modulation when required, provided by the external delay–lines (fig. 1) or the turbulence itself [21]. Indeed, when fringes move at least a few λ, which is the case during fringe search, averaging $(A-C)^2+(B-D)^2$ or $(A-C)^2$ resume to the same operation in the photon–noise regime. $\langle S^2 \rangle$ measured with FSU_1 is even better for fringe detection than $\langle V^2 \rangle$ measured with FSU_0 since FSU_1 is more efficient for modulation and detection. A similar scheme can be used for chromatism measurement if the dynamic of $S(\sigma)$ is insufficient in each spectral channel.

Coherencing with only one dispersed output has been reminded in section 1.2. But the channeled spectrum algorithm is blind at L_a=0. Fig. 4c shows that the $DFT_{K,K'}$ algorithm also suffers from sign indetermination when used with two outputs (K=2) since the two fringe peaks are on the same line. It thus seems impossible to derive a monotonous OPD estimator with FSU_1. Yet, assuming sine fringes, fig. 4c shows that changing the OPD sign changes the fringe pattern. The OPD sign should thus be derived with relevant processing. In fact, the sign information lies in the phase of the fringe peak. But when the DFT is performed in the $[\sigma_1, \sigma_2]$ spectral window, the phase information is not directly usable and is discarded by usual algorithms. This is clearly shown by fig. 7: changing the OPD changes the fringe frequency, the phase reference point being located at σ=0.

Therefore, using the $[0, \sigma_2]$ window, the phase of the fringe peak is $\pm\pi/2$ according to the OPD sign, whereas the modulus gives the OPD amplitude. This only works for sine fringes and justifies the emphasize put on Φ_r in this paper (appendix A). The window can also be increased using negative wavenumbers: Eqs. (1) and (7) show that changing the sign of σ is equivalent to adding π to the modulation phase. The bidimentionnal $[\{0, \pi\}, \sigma]$ interferogram of FSU_1 can then be changed to a monodimensional $[-\sigma, +\sigma]$ interferogram and processed by a 1D–DFT as shown in fig. 7. With this algorithm, the resolution of the estimated OPD is higher since the width of the spectral window is increased. But since the DFT is performed on a window wider than the data support, the fringe peak is enlarged (convolution by a sinc). However the same phenomenum (spectral leakage) applies, with a lower magnitude, to any DFT algorithm when the number of fringes in the spectrum is not an integer. Since the shape of the interferogram is known (sinus with unknown signed frequency), another demodulation algorithm should be used. The result with least–square fitting (fig. 3b, dotted line) shows that a very good OPD resolution is achievable at high SNR.

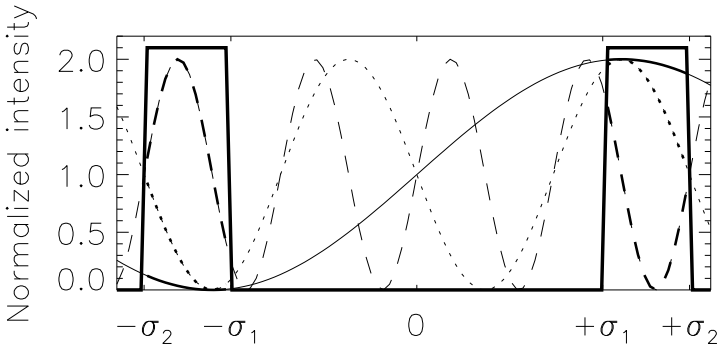

Figure 7. Normalized extended spectral interferogram and analysis window (thick, $\sigma_1^{-1} = 2.4$ μm, $\sigma_2^{-1} = 1.5$ μm) for L_a=0.5 μm, (—), 3 μm (- - -), -1.5 μm (...).

Dispersing the two outputs of a BS seems thus to be an efficient coherencing setup. First, all the light is used. Second, it makes full use of the *a priori* knowledge (sine fringes), allowing OPD estimation with sign (full dynamic) and resolution. Tracking can thus occur at L_a=0 where the fringe contrast is maximum. Third, detector noise is lower than with the $DFT_{4,K'}$ algorithm since the number of pixels per channel is lower. This algorithm can even be refined to take into account variation of the fringe parameters in the spectral channels such as instrumental chromatism, the actual prism dispersion, or *a priori* knowledge of the OPD temporal evolution [22]. This algorithm can at least be used for simultaneous coherencing in a cophasing mode, where noise is negligible. Detailled analysis of pure coherencing at low SNR is under investigation and should be the subject of a next paper.

2.4. The FSU_2 concept (SI)

In a SI, measurements are most often spectrally resolved and may be made for each polarization. Even with OPD stabilization, the phase of the fringes Φ may not be 0 in each spectral channel because of OPD residuals, chromatic effects or object phase. Full demodulation with at least $K \geq 3$ samples is most often required in a SI.

As previously made with DFT_2, the best implementation of DFT_K algorithm should use an achromatic discrete spatial modulation with K simultaneous outputs $2\pi/K$ phase–shifted. Similar devices have already been proposed [7, 23], based on a chromatic modulation or assuming a constant phase over the pupil. Although the best setup should use K=3 samples to minimize detector noise, a simple implementation can be derived for K=4 based on the direct measurement of the sine quadrature by FSU_1. The cosine quadrature can be derived by feeding another FSU_1 with half the light, with an additionnal $\pi/2$ phase shift between arms 1 and 2. A simpler solution is to carry each quadrature on a polarization within the same FSU_1 and to insert a polarization shift Φ_p=$\pi/2$ in one arm [20]. This polarization shift can be done with a total reflection at incidence i between media of index n and 1 [24, 25] (fig. 8):

$$\tan\left(\frac{\Phi_p}{2}\right) = \frac{\cos i\sqrt{\sin^2 i - 1/n^2}}{\sin^2 i}. \tag{11}$$

Since n changes slowly with wavelength, Φ_p is nearly achromatic. A classical application is the Fresnel prism, introducing a 90 ° shift with a double reflection at i=55 ° in a $n \simeq 1.5$ glass [24, 25].

FSU_2 (fig. 9) is a SI based on this principle, derived from FSU_1. The BS and the folding mirror in fig. 6 are replaced by an assembly of three identical prisms P_1, P_2 and P_3, cut from the same plate and optically contacted together with a BS inserted between P_2 and P_3 [24]. Equal paths in prisms P_1+P_2 and P_3 ensures glass compensation. Using ZnSe ($n \simeq 2.45$), the total reflection R at incidence i=33 ° introduces a polarization phase shift varying between 89.4 ° and 90.05 ° in the spectral band [1.5,5] μm. The exact value of the phase shift can be used in each spectral channel to improve demodulation. FSU_2 assumes that polarizations have the same V and Φ parameters. If not, FSU_2 can be fed with a single linear polarization at 45 ° incidence for accurate measurements. Since filtering occurs after beam combination, η_s can be estimated by statistical means [5, 26].

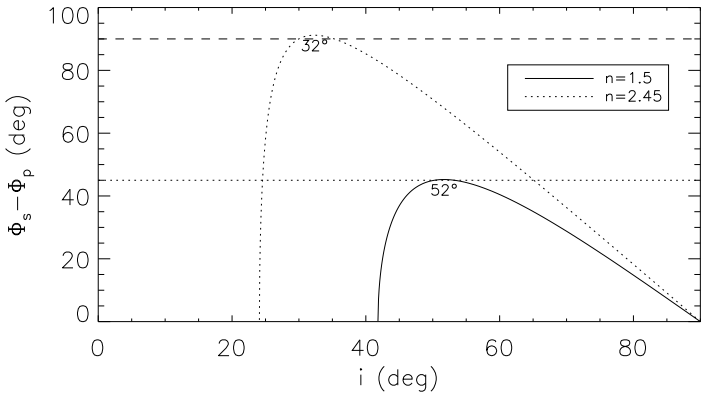

Figure 8. Phase shift between polarizations occurring at total reflection. The incidence i at maximum is indicated.

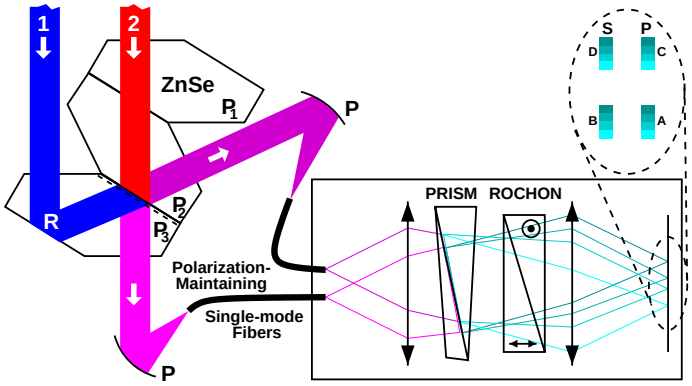

Figure 9. FSU_2 concept: the BS of FSU_1 (fig. 6) is replaced with a prism assembly $P_{1,2,3}$ creating an achromatic $\pi/2$ phase shift between polarizations at total reflection R. Quadratures are jointly transmitted with polarization maintaining fibers and split before detection with a Rochon prism.

2.5. Combining more than two beams

With N_B beams, there are $N_B(N_B-1)/2$ baselines of interest for the SI, but only N_B-1 relevant OPDs to measure in the OS, at the shortest baselines for higher visibility. Separating the OS and the SI is thus even more justified.

An efficient three–beam FSU is based on pupil shearing [27]. This setup delivers 3 pairs of complementary outputs, as FSU_1. But the double–pass through the BS leads to cosine fringes forbidding coherencing at OPD=0. This setup can be used as a SI to measure phase closures with an additional modulation. Since it must be compensated for polarization phase shifts, a polarization–based (achromatic) modulation may be done as in FSU_2.

3. SIMULATED PERFORMANCE

The three FSUs presented in section 2 have been compared in a pure cophasing mode (α=1) by a simulation including photon, detector and turbulence noises. Two files of AO–corrected wavefronts were first generated for bad conditions at Paranal (r_0=10 cm at 0.5 μm, m_V=17.5 guide star, diameter=8 m, sampling frequency f=2.5 kHz, 55 Zernike modes corrected). These files were then converted into complex amplitude E_i in the H band by projection on a Gaussian mode. The same detector was used for all FSUs. For FSU_0, a single output of the BS and 4 successive samples with a $\pi/2$ OPD step are used and proceeded with Eq. (3). For FSU_1, 4 successive samples are binned together on each output and then proceeded with Eq. (4) to deliver S and $\widehat{\Phi}$ at the same frequency $f/4$. A similar scheme is used for FSU_2. No polarization or chromatism are assumed. To evaluate only the measurement noise, the interference was made with $|E_i|$ to get rid of the additional piston introduced by filtering and L_a=0.

Results are plotted on fig. 10 (rising curves with full symbols), clearly showing the photon and detector noise regimes discussed with Eq. (5). A saturation regime is evidenced at low flux where Eq. (5) is no longer valid since $\widehat{\Phi}$ tends towards a white noise in $]-\pi,\pi]$ of standard deviation $2\pi/\sqrt{12}$. Cophasing is then impossible because of fringe jumps. Since the limiting cophasing magnitude is in the detector noise regime, FSU_1 is at least twice better than FSU_2 and four times better than FSU_0. Scintillation noise introduced by temporal modulation is evidenced by FSU_0 at low magnitude.

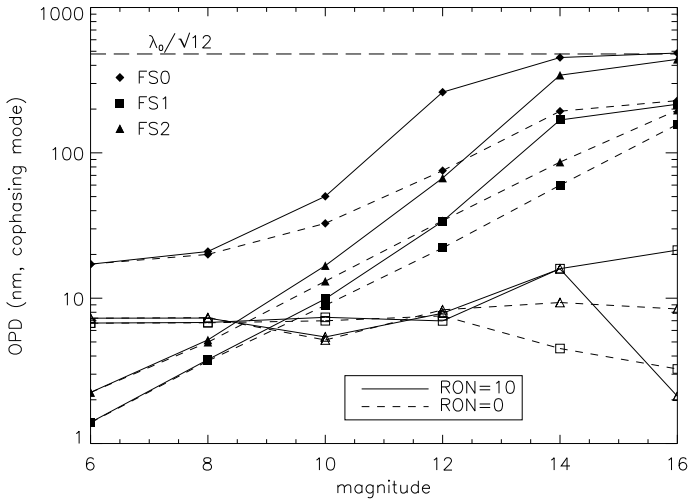

Figure 10. Performance simulation of FSU_0, FSU_1 and FSU_2 in the cophasing mode. The standard deviation of the OPD estimator (S or $\widehat{\Phi}$, full symbols) and the bias for a 5% transmission error in one arm (empty symbols) are plotted for two read–out noise (RON) σ_e values.

In a second step, a constant 95% transmission has been introduced in one arm to simulate an important calibration error (fig. 10, flat curves with open symbols). This calibration noise is most often negligible, and lower than the scintillation noise introduced by temporal modulation in FSU_0.

SUMMARY AND CONCLUSION

The best strategy for fringe sensing in stellar interferometry has been investigated. Since the OS and the SI have different requirements (resp. short/long exposure, 1/2 quadrature demodulation, no or small/good spectral resolution, $N_B - 1/N_B(N_B-1)/2$ pairs combination), they should *a priori* be distinct but use the same spatial filter to see the same OPD with large pupils and partial AO correction. All the spectral domain or polarization of interest can then be sent to the SI, leaving all the remaining part of the light for the OS.

Our analysis shows that a linear achromatic spatial discrete modulation with K=2 (OS) or $K \in \{3,4\}$ (SI) samples maximizes instrumental visibility, minimizes detector noise, and allows demodulation in each chromatic channel by the DFT algorithm with minimum noise propagation. Calibration noise introduced by spatial modulation is most often negligible and smaller than scintillation noise introduced by temporal modulation.

Two conceptual designs FSU_1 and FSU_2 based on this principle are described and compared with the classical FSU_0 concept. FSU_1 and FSU_2 do not require high–frequency moving parts which is a definite advantage for future space missions. Other implementations can be foreseen, using integrated optics [17] or STJ detectors with intrinsic spectral resolution [28].

FSU_2 can be used as a SI with better performance than FSU_0. FSU_1 is an OS optimized for fringe tracking in the cophasing mode, with simultaneous coherencing by a new algorithm. We expect it to be also very efficient in the pure coherencing mode at low SNR, under investigation. FSU_1 can also be used for fringe detection, visibility or chromatism measurement before tracking using the external delay–line or the atmospheric turbulence. Simulations confirm that FSU_1 is the best OS for cophasing.

ACKNOWLEDGMENTS

The authors would like to thank J. Gay and S.Menardi for fruitful discussions and P. Dierich for pointing out ref. [24].

APPENDIX A. BEAM COMBINATION AND REFERENCE PHASE

Two methods, wavefront and amplitude division, can be considered for beam splitting or combining [25]. Three interferometer types can thus be distinguished (fig. 11): the Young interferometer (a) based on wavefront division and combination, the Mach Zehnder interferometer (c) based on amplitude division and combination, and the mixed case (b) with one of each.

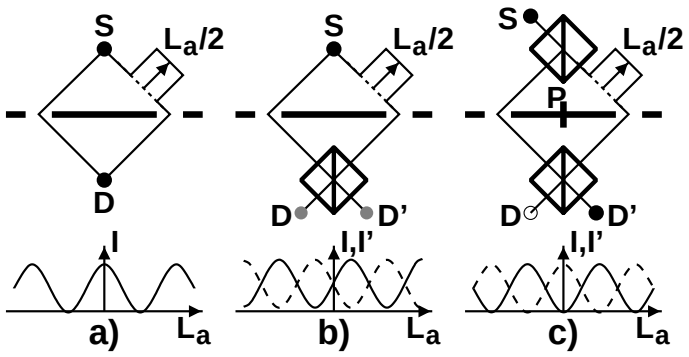

Figure 11. Young (a), mixed (b) and Mach Zehnder (c) interferometers. The source is located in S and the detectors in D and D'. Their intensity I and I' is plotted versus the OPD L_a between the beams.

Let us suppose that the two arms have equal length when L_a=0. In the Young case, it is obvious by symmetry around (SD) that constructive interference occurs on the detector D. The intensity I is thus maximum. In the mixed case, there are two outputs D and D'. If the beam splitter is non absorbing, these two outputs are complementary for energy conservation. Therefore, by symmetry, I and I' are equal for L_a=0. In the Mach Zehnder case,the central symmetry around point P makes the intensity maximum at D' and null at D.

This shows that for the same OPD L_a, the phase of the fringes differs with the type of interferometer. It can be shown that the reflection and transmission coefficients in a BS are in quadrature [29, 30]. Most laboratory interferometers use similar methods for beam splitting and combining (fig. 11a, c), leading to cosine fringe when varying the OPD between the beams, *i. e.* $\Phi_r=\pi/2$ in Eq. (1). But the mixed case leads to sine fringes, *i. e.* $\Phi_r=0$ in Eq. (1). This phase reference Φ_r is distinguished from the instrument phase Φ_i because Φ_r is achromatic in the Young case and can be controlled in a BS by careful design of the semi–reflective [30] and antireflection [31] coatings, or by evanescent–wave coupling [32].

REFERENCES

1. P. Lawson, ed., *Selected papers on Long Baseline Stellar Interferometry*, vol. MS 139 of *SPIE Milestone Series*, SPIE Optical Engineering Press, 1997.
2. R. D. Reasenberg, ed., *Astronomical Interferometry*, no. 3350 part II in Proc. Soc. Photo-Opt. Instrum. Eng., Proc. Soc. Photo-Opt. Instrum. Eng., 1998.
3. M. Shao, M. M. Colavita, B. E. Hines, D. H. Staelin, D. J. Hutter, K. J. Johnston, D. Mozurkewich, R. S. Simon, J. L. Hershey, J. A. Hughes, and G. H. Kaplan, "The Mark III Stellar Interferometer," *Astron. Astrophys.* **193**, pp. 357–371, 1988. Also in [1].
4. J. T. Armstrong *et al.*, "The NAVY prototype optical interferometer," *Astrophys. J.* **496**, pp. 550–571, Mar. 1998.
5. M. M. Colavita *et al.*, "The palomar Tested Interferometer," *Astrophys. J.* **510**, pp. 505–521, Jan. 1999.
6. A. Glindemann *et al.*, "The VLTI – The observatory of the 21st century," *The ESO Messenger* **98**, pp. 2–7, Dec. 1999.

7. A. Quirrenbach *et al.*, "PRIMA – Study for a dual-beam instrument for the VLT Interferometer," in Reasenberg [2], pp. 807–817.
8. B. Sorrente, F. Cassaing, G. Rousset, S. Robbe, and Y. Rabbia, "Real-time optical path difference stabilization by ASSI at the I2T interferometer," *Astron. Astrophys.* , submitted.
9. F. Cassaing, *Analyse d'un instrument à synthèse d'ouverture optique : méthodes de cophasage et imagerie à haute résolution angulaire.* PhD thesis, Université Paris XI Orsay, Dec. 1997.
10. S. Lévêque, B. Koehler, and O. von der Lühe, "Longitudinal dispersion compensation for the Very Large Telescope Interferometer," *Astrophys. Space. Sci.* **239**(2), pp. 305–314, 1996.
11. C. Dessenne, P. Y. Madec, and G. Rousset, "Optimization of a predictive controller for closed-loop adaptive optics," *Appl. Opt.* **37**, pp. 4623–4633, July 1998.
12. L. Kœchlin, P. R. Lawson, D. Mourard, A. Blazit, D. Bonneau, F. Morand, P. Stee, I. Tallon-Bosc, and F. Vakili, "Dispersed fringe tracking with the multi-r_o apertures of the Grand Interféromètre à 2 Télescopes," *Appl. Opt.* **35**, pp. 3002–3009, June 1996.
13. P. R. Lawson, "Group delay tracking in optical stellar interferometry using the Fast Fourier Transform," *J. Opt. Soc. Am. A* **12**, pp. 366–374, 1995.
14. G. Rousset, P. Y. Madec, and D. Rabaud, "Adaptive optics partial correction simulation for two telescope by interferometry II," in *High Resolution Imaging*, No. 39, pp. 1095–1104, ESO, (Garching, Germany), 1991.
15. P. Connes, C. Froehly, and P. Facq, "A fiber-linked version of project TRIO," in *Colloquium on kilometric optical arrays in space*, No. 226 in SP, pp. 49–61, European Space Agency, Oct. 1984.
16. E. G. Neumann, *Single-mode fibers*, Springer-Verlag, 1988.
17. F. Malbet *et al.*, "Integrated optics for astronomical interferometry I. concept and astronomical applications," *Astron. Astrophys. Suppl. Ser.* **138**, pp. 1–10, 1999.
18. C. Ruilier and F. Cassaing, "Coherent coupling through turbulence: application to stellar interferometry," *J. Opt. Soc. Am. A* , submitted.
19. V. Coudé du Foresto and S. Ridgway, "FLUOR: a stellar interferometer using single-mode infrared fibers," in Beckers and Merkle [33], pp. 731–740. Also in [1].
20. Y. Rabbia, S. Menardi, , F. Reynaud, and L. Delage, "The ESO-VLTI fringe sensor," in *Astrofib'96 : Integrated optics for astronomical interferometry*, P. Kern and F. Malbet, eds., pp. 175–183, (Grenoble), Oct. 1996.
21. W. J. Tango and R. Q. Twiss, "Michelson stellar interferometry," in *Progress in Optics*, E. Wolf, ed., vol. XVII, ch. IV, p. 239, North Holland Publishing Company - Amsterdam, 1980. Also in [1].
22. L. Kœchlin, "Interférométrie stellaire dans l'espace : détection des franges," *J. of Optics (Paris)* **16**(6), pp. 269–276, 1985.
23. E. Serabyn, "Nanometer–level path–length control scheme for nulling interferometry," *Appl. Opt.* **38**, pp. 4213–4216, July 1999.
24. P. Juncar, M. E. H. H. Elandaloussi, J. Pinard, and A. Razet, "A new optical wavelength ratio measurement apparatus: the fringe counting sigmameter," *IEEE Trans. Instrum. Meas* **46**, pp. 690–695, June 1997.
25. M. Born and E. Wolf, *Principles of Optics*, Pergamon Press, 1993.
26. S. B. Shaklan, M. M. Colavita, and M. Shao, "Visibility calibration using single mode fibers in a long-baseline interferometer," in Beckers and Merkle [33], pp. 1271–1283.
27. F. Roddier, "Ground–based interferometry with adaptive optics," in *Working on the Fringe*, Astronomical Society of the Pacific, (Dana Point), May 1999.
28. A. Peacock, P. Veerhoeve, N. Rando, A. van Dordrecht, B. G. Taylor, C. Erd, M. A. C. Perryman, R. Venn, J. Howlett, D. J. Coldie, J. Lumley, and M. Wallis, "Single optical photon detection with a superconducting tunnel junction," *Nature (London)* **381**, pp. 135–137, May 1996.
29. D. Mékarnia and J. Gay, "Infrared multispectral interferometry," *Astron. Astrophys.* **238**, pp. 469–474, 1990.
30. J. D. Phillips and C. Hickey, "Beamsplitters for astronomical interferometry," in *Spaceborne Interferometry II*, R. D. Reasenberg, ed., vol. 2477, pp. 132–148, Proc. Soc. Photo-Opt. Instrum. Eng., Apr. 1995.
31. F. Lemarquis, A. Fornier, and E. Pelletier, "Compensation of phase shitf induced by beam-splitter plate and compensating plate coatings in a Michelson-type interferometer," *Pure Appl. Opt.* **4**, p. 185, 1995.
32. J. M. Thériault, "Modeling the responsivity and self-emission of a double-beam Fourier-transform infrared interferometer," *Appl. Opt.* **38**, pp. 505–515, Jan. 1999.
33. J. M. Beckers and F. Merkle, eds., *High resolution imaging by interferometry II, part II: multiple aperture interferometry*, no. 39 in Proceedings ESO, NOAO-ESO, Oct. 1991.